Two-Dimensional Superstructure Formation of Fluorinated Fullerene on Au(111): A Scanning Tunneling Microscopy Study

Tomoko K. Shimizu,[†,⊥] Jaehoon Jung,[†,⊥] Tetsuya Otani,[†,‡] Young-Kyu Han,[§] Maki Kawai,[‡,*] and Yousoo Kim[†,*]

[†]RIKEN Advanced Science Institute, 2-1 Hirosawa, Wako, Saitama 351-0198, Japan, [‡]Department of Advanced Materials Science, The University of Tokyo, 5-1-5 Kashiwanoha, Kashiwa, Chiba 277-8561, Japan, and [§]Division of Materials Science, Korea Basic Science Institute, Daejeon 305-333, Republic of Korea. [⊥]These authors contributed equally to this work.

ABSTRACT

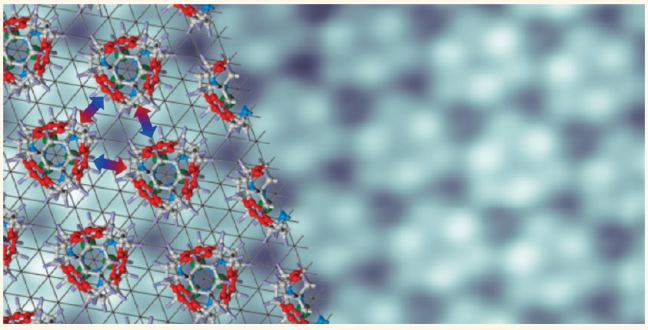

A two-dimensional fluorinated fullerene ($C_{60}F_{36}$) superstructure has been successfully formed on Au(111) and was investigated using scanning tunneling microscopy (STM) and density functional theory calculations. Although there exist three isomers (C_3, C_1, and T) in our molecular source, STM images of the molecules in the well-ordered region all appear identical, with 3-fold symmetry. This observation together with the differences in the calculated lowest unoccupied molecular orbital (LUMO) distribution among the three isomers suggests that a well-ordered monolayer consists of only the C_3 isomer. Because of the strong electron-accepting ability of $C_{60}F_{36}$, the adsorption orientation can be explained by localized distribution of its LUMO, where partial electron transfer from Au(111) occurs. Intermolecular C—F···π electrostatic interactions are the other important factor in the formation of the superstructure, which determines the lateral orientation of $C_{60}F_{36}$ molecules on Au(111). On the basis of scanning tunneling spectra obtained inside the superstructure, we found that the LUMO is located at 1.0 eV above the Fermi level (E_F), while the highest occupied molecular orbital (HOMO) is at 4.6 eV below the E_F. This large energy gap with the very deep HOMO as well as uniform electronic structure in the molecular layer implies a potential for application of $C_{60}F_{36}$ to an electron transport layer in organic electronic devices.

KEYWORDS: fluorinated fullerene · scanning tunneling microscopy · density functional theory · electron acceptor · charge transfer · C—F···π interaction

Fluorination is an established technique for tuning the electronic and optical properties of organic molecules by stabilizing the energy levels of frontier orbitals.[1−4] The resulting molecules thus exhibit higher electron affinity (EA) than do their original nonfluorinated forms due to the strong electron withdrawal of fluorine atoms.[5,6] In organic devices such as field effect transistors, the increase in EA leads in principle to a decrease in the electron injection barrier at the interface between the molecular film and the metal electrode, yielding n-type semiconducting behavior.[7] A better understanding of the structural and electronic properties of thin films of fluorocarbons deposited on metals is therefore considered essential for further advances in organic electronics.

The fluorinated fullerene, $C_{60}F_x$, is a useful fluorocarbon from this perspective. The "surface transfer doping" effect[8] has been observed on a hydrogen-terminated insulating diamond surface as a result of effective charge transfer between diamond and the molecules, producing a conduction layer on the diamond surface.[9−11] As the number of added fluorine atoms x increases, the EA of $C_{60}F_x$ and thus electron-accepting ability increase accordingly.[12] Several spectroscopic studies of $C_{60}F_x$ (x = 18, 36, and 48) films have found that while the lowest unoccupied molecular orbital (LUMO) does not change significantly,[13] the reduction of π states due to the decrease in the number of C=C bonds appears as a decrease in intensity or as a disappearance of the highest occupied molecular orbitals (HOMO) and HOMO−1. As a result, the HOMO level shifts to a point far deeper than the Fermi level (E_F).[14] However, the details of adsorption and electronic structures at the interface between metals and films of fluorinated fullerenes have not yet been clarified because of their structural complexity as well as the presence of isomers. Therefore, it is desirable to obtain microscopic information on their monolayers deposited on metal substrates.

In most cases of fluorination, hydrogen atoms are substituted with fluorine atoms, barely affecting the molecular structure.[15] Fluorination of the fullerene, by contrast,

* Address correspondence to ykim@riken.jp (Y.K.); maki@k.u-tokyo.ac.jp (M.K.).

Received for review January 6, 2012 and accepted February 13, 2012.

Published online February 13, 2012
10.1021/nn300064x

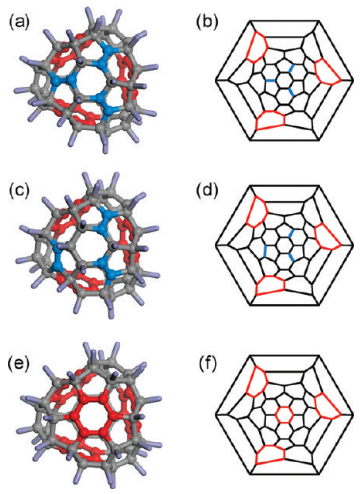

Figure 1. Optimized structures (a, c, e) and Schlegel diagrams (b, d, f) for C_3 (a and b), C_1 (c and d), and T (e and f) $C_{60}F_{36}$ isomers. Nonfluorinated moieties (phenyl rings and C═C bonds) are colored red and blue (respectively).

results from the addition of two fluorine atoms per C═C bond, causing a change in the bonding configuration of the carbon atoms from sp^2 to sp^3, which changes the molecular structure of the spherical C_{60} moleule.[16,17] Due to their complex shape and the presence of F atoms at the periphery, different types of intermolecular interactions than van der Waals interaction are expected, which may result in unique molecular packing. For instance, it has been reported that the molecular packing and the growth mode of perfluoropentacene films are very different from those of pentacene films even though their molecular structures are not significantly different.[7,18,19]

In this article, we report the successful fabrication and detailed analysis of a well-ordered one-monolayer film made of one of the fluorinated fullerenes, $C_{60}F_{36}$, on Au(111) using scanning tunneling microscopy (STM) and density functional theory (DFT) calculations. Although $C_{60}F_{36}$ has three isomers, C_3, C_1, and T (Figure 1),[20] a well-ordered molecular monolayer consists of only the C_3 isomer, which is reasonably suggested by (i) the highly symmetric and 3-fold STM images for the molecules adsorbed on Au(111), (ii) the difference in orbital distribution of the C_3 isomer from those of other isomers, and (iii) the abundance of the C_3 isomer compared to others (C_3:C_1:T = 70:25:5).[20] We found that there is an intermolecular electrostatic interaction between the fluorinated moieties (C−F) and the nonfluorinated moieties (π states of phenyl rings) of adjacent molecules. This type of C−F$\cdots\pi$ interaction has been reported only for 3D crystals of fluorocarbons.[17,21−24] Scanning tunneling spectroscopy (STS) revealed that the molecular layer possesses a large band gap (>5 eV) with its LUMO much closer to the E_F than its HOMO, implying that the majority carrier in the film is electrons.

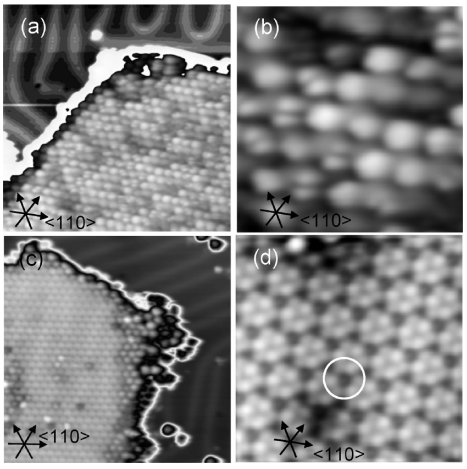

Figure 2. STM images of $C_{60}F_{36}$ on the Au(111) surface. (a and b) $C_{60}F_{36}$ island formed by depositing molecules onto Au(111) kept at room temperature, producing a number of islands consisting of inhomogeneous regions. (c and d) $C_{60}F_{36}$ island created in the same way as in (a) and (b) followed by annealing to 370 K, resulting in the formation of the homogeneous regions. Image sizes of (a) and (c) are 30 × 30 nm^2; (b) and (d) 6 × 6 nm^2. Color scale in (a) and (c) is not linear to enhance the contrast of both molecules inside the islands and the herringbone structure of bare Au(111). Tunneling parameters in (a) and (b) are V_{sample} = 2.4 V and I_t = 0.14 nA; in (c) and (d) V_{sample} = 2.4 V and I_t = 0.20 nA.

RESULTS AND DISCUSSION

Deposition of $C_{60}F_{36}$ by sublimation of a powder source onto the Au(111) surface at room temperature initially led to step edge decoration. As the amount of deposited molecules increased, islands grew from the lower step edges to the terraces. Figure 2a is a typical STM image of such an island. It is composed of grainy spots with various types of intramolecular structures, as shown in the enlarged image in Figure 2b. We refer to such an area as an "inhomogeneous region". The distance between two adjacent molecules was 1.11 ± 0.04 nm. Differences in appearance may be related to the orientation of the molecules as well as to the different types of isomers.

When we annealed the sample to 340−370 K after molecular deposition, almost all the molecular islands showed areas within which there was very little height variation, although others and the perimeters of the islands still corresponded to the inhomogeneous region, as shown in Figure 2c. We call such uniform, less corrugated areas "homogeneous regions". An enlarged image is shown in Figure 2d. The periodicity of this region was 1.15 ± 0.08 nm, very similar to the lattice constant in the inhomogeneous region. By enhancing the contrast inside the molecular island (Figure S1), we confirmed that the herringbone reconstruction was preserved under the molecular islands. It is thus unlikely that Au vacancies are created by annealing, which has been reported for the C_{60} monolayer on Au(111), but this occurred when the surface was annealed to as high as 540[25] and 680 K.[26]

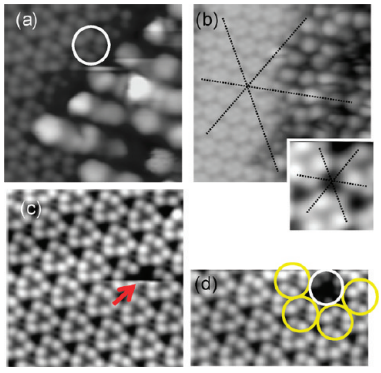

Figure 3. (a and b) STM images of the boundary region. The circled unit in (a) corresponds to a single molecule. The three dotted lines in (b) are lattice lines, and an enlarged image of the intersection is shown in the inset. (c) During and (d) after the STM tip interacted with a molecule indicated by a red arrow in (c). This merely resulted in a change in appearance to the white circled molecule in (d), which is darker than neighboring molecules (yellow). Slow scan direction is from the bottom to the top. Tunneling conditions in (a) and (b) were $V_{sample} = 2.4$ V and $I_t = 0.20$ nA; in (c) and (d) $V_{sample} = 2.8$ V and $I_t = 0.30$ nA. Image size: (a) 6×6 nm^2; (b) 10×10 nm^2; (inset) 1.2×1.2 nm^2; (c) 6×6 nm^2; (d) 6×3.2 nm^2.

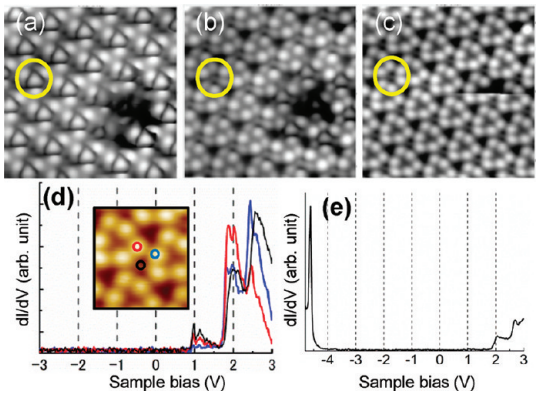

Figure 4. (a−c) Bias dependence of STM images acquired at $I_t = 0.30$ nA and $V_{sample} = 1.2$ V (a), 2.0 V (b), and 2.8 V(c). Image size is 6×6 nm^2. Circled unit in each image is the single molecule. (d) Scanning tunneling spectra (STS) obtained at three distinct positions of the molecule. Colors in the image and spectra correspond to each other. Feedback was open at $V_{sample} = 2.7$ V and $I_t = 0.30$ nA. Inset image (1.85×2 nm^2) was obtained with $V_{sample} = 2.8$ V and $I_t = 0.30$ nA. (e) STS with wider bias range. Feedback was open at $V_{sample} = 2.8$ V and $I_t = 0.20$ nA.

Appearance of the herringbone structure within the molecular island also excludes the possibility that the sample annealing results in F atom detachment from the molecules, and detached F atoms migrate under the molecular island as observed for annealed $C_{60}F_{48}$/graphene/SiC.[27] Direct bonding of F and Au atoms would lift the reconstruction. Neither did we find any dark spots on the bare Au(111) area that could be attributed to migrated F atoms, which have been observed on Si(111)-(7×7).[28,29]

With a larger scale STM image that contains both a molecular island and a large area of the bare Au(111) surface (Figure S1), we could easily recognize that one of the close-packed directions of the molecular island is perpendicular to the parallel lines of the herringbone structure, *i.e.*, along the ⟨110⟩ direction. This fact was used for constructing the superstructure model, which will be shown later.

We found that the repeat unit, shown circled in Figure 2d, corresponded to a single $C_{60}F_{36}$ molecule, which exhibited 3-fold symmetry. This conclusion is based on the following observations. First the boundary between the homogeneous and inhomogeneous regions (Figure 3a) clearly shows that the triangular unit cannot be a single molecule, as it is unlikely to break chemical bonds of all molecules at the boundary. If we simply assume that all molecules are intact, a unit circled in the solid line must correspond to the single molecule. Second, we found that three lattice lines drawn from the inhomogeneous region to the homogeneous region (Figure 3b) intersected at the dark spots (enlarged image shown in the inset of Figure 3b), which should correspond to the center of a molecule in the homogeneous region. Third, we found while scanning that the STM tip interacted with one of the molecules and its appearance suddenly changed (Figure 3c and d). This could be attributed to desorption (*i.e.*, the molecule disappeared from the surface) or chemical reaction that transformed the electronic structure of the molecule dramatically. From this observation it would appear that the single molecule most likely corresponds to the circled units.

As already seen in Figures 2 and 3, each molecule consists of a dark spot at the center and six bright lobes, three of which are brighter than the others. Relative brightness, however, changes depending on the applied bias voltage, as shown in Figure 4a−c. At low sample bias voltages (Figure 4a), the center of the molecule appears as a bright spot. As the bias increases (Figure 4b), the center becomes darker, and further increase of the bias results in six lobes having similar brightness (Figure 4c). STS of three distinct sites of the molecule are shown in Figure 4d. Although there are differences in intensities, peak positions are almost equal, meaning that the electronic structure of the monolayer film is quite uniform.

At all bias voltages explored, the molecule showed 3-fold symmetry. Therefore, we expect that the $C_{60}F_{36}$ in the homogeneous region is adsorbed in such a way that the 3-fold symmetry axis is perpendicular to the Au(111) surface. There are two possible orientations for the C_3 and T isomers that satisfy this criterion and none for the C_1 isomer, which may exclude the possibility of involvement of the C_1 isomer in the homogeneous region. Figure 5 shows the optimized structures of three isomers in the gas phase (a) and their LUMO distributions (b) from both side and bottom views. The electronic structures of the isomers strongly depend on the location of the fluorine atoms, *i.e.*, the resultant

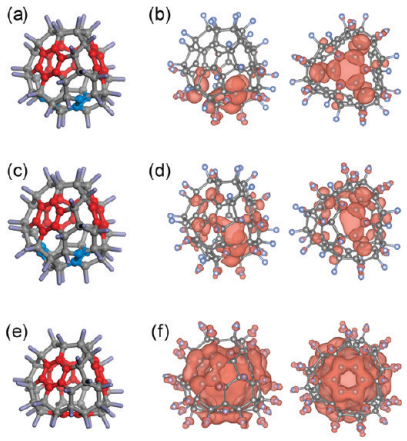

Figure 5. Optimized structure in the gas phase (a, c, e) and side (left) and bottom (right) views of their LUMO (b, d, f) for the C_3 (a and b), C_1 (c and d), and T (e and f) isomers. Nonfluorinated moieties (phenyl rings and C═C bonds) are colored red and blue, respectively. For clear comparison with the STM image, the LUMO distribution is described as the square of the molecular orbital, which represents the relative probability of finding an electron in the molecule. For the T isomer, the three degenerate molecular orbitals are merged to depict the LUMO distribution. Isosurface value is 0.001 e/bohr.[3]

changes in the symmetry of the isomers. The LUMO spatial distributions of C_3 and C_1 isomers are clustered predominantly around three C═C bonds, whereas that of the T isomer is triply degenerated and distributed on the four phenyl moieties. The bottom view of the LUMO more clearly shows that the LUMO distribution of the C_1 isomer cannot yield 3-fold symmetry in the STM images at low bias voltages, as shown in Figure 4a.

In general, the spatial distribution of frontier molecular orbitals is considered to be a decisive parameter in the stability and relative orientation of chemical species that interact with each other via charge transfer.[30−32] Evaluation of the LUMO distribution is particularly important in the case of $C_{60}F_{36}$ because of its high EA,[6] implying that the LUMO tends to approach the E_F of Au(111).[2] In fact, we found the highest occupied state at −4.6 V below the E_F, while the lowest unoccupied state was at +1.0 V (Figure 4e); that is, the center of the HOMO and LUMO that can be regarded as the molecular E_F in the gas phase[33,34] goes downward upon adsorption with respect to the E_F of the substrate. This suggests an additional electronic charge in the molecule as a result of partial electron transfer from Au(111) to the molecule.[35,36] Therefore, it is likely that the orientation of the C_3 isomer is such that the part where the LUMO is distributed is oriented toward the Au(111) surface.[37−39] Periodic DFT calculations for the C_3 and T isomers including the Au(111) substrate were performed to investigate the adsorption orientation and charge transfer between the molecule and the substrate. On the basis of the intermolecular distance, 1.15 ± 0.08 nm, measured from the molecularly resolved STM images, the periodicity of the superstructure was determined to be (4 × 4). Figure 6 shows the optimized

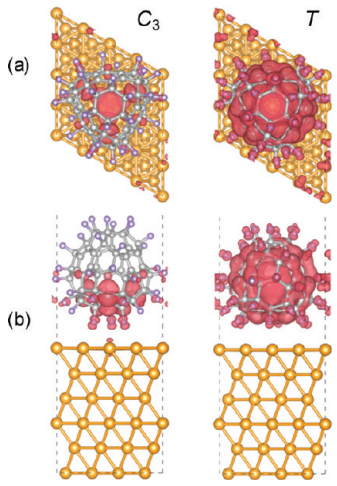

Figure 6. Top views (a) and side views (b) of the LUMO distribution of C_3 and T isomers adsorbed on the top site of Au(111). Isosurface value is 0.0015 e/bohr.[3]

structures of the C_3 and T isomers adsorbed on the Au(111) substrate (see also Figure S2 for detailed geometry). As expected, the configuration with the C═C bond side down, where the LUMO of the C_3 isomer faces the substrate, is more stable by 0.07 eV than the opposite orientation (C═C bond side up) when the molecule is adsorbed on an Au(111) top site. The Bader population analysis revealed that 0.36e was transferred from Au(111) to a single $C_{60}F_{36}$ molecule. This value is larger than that for C_{60}/Au(111), 0.2e per molecule,[40] evaluated using a similar calculation method. The increase in the amount of electron transferred indicates the increase in electron-accepting ability by fluorination. The T isomer, at a similar orientation with one of the four phenyl rings at the bottom side, was found to be more stable by 0.17 eV than in the upside-down orientation.

We further found that the calculated spatial distributions of the LUMO for both C_3 and T isomers are quite different from each other (Figure 6). As shown above, the molecules in the homogeneous region all appear identical, and therefore, we strongly believe that the region consists of only one type of isomer. On the basis of the isomer ratio, it is likely that the homogeneous region is comprised of the C_3 isomer because we found experimentally that the area of the homogeneous region accounts for more than 60% of the entire area covered by molecules (Figure S1). Indeed, the spatial distribution of the LUMO of the C_3 isomer resembles the STM image at low bias (Figure 4a). Higher MOs for the C_3 isomer (Figure S3a) can also explain well the experimentally observed bias dependence of the STM images (Figure 4). At low bias, the molecular center and phenyl ring parts are expected to be bright (779 and 780 states), and as the bias increases, C_6F_6 parts are also expected to appear bright (784 + 785 state). In contrast, all major MOs for the T isomer (Figure S3b) are distributed around phenyl rings, which cannot explain the bias dependence of the STM images.

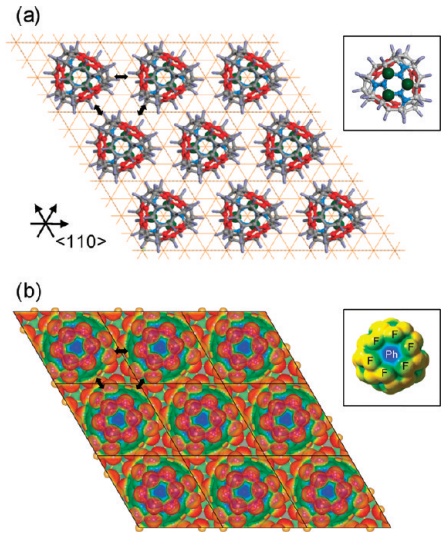

Figure 7. (a) (4 × 4) superstructure model for the homogeneous region of the $C_{60}F_{36}$ monolayer on Au(111). Three fluorine atoms at the bottom bonded to Au are emphasized in size and color (green) to clearly show the adsorption sites. Solid yellow lines show the gold lattice. Inset is the bottom view of the single molecule of the C_3 isomer. (b) Calculated electrostatic potential (ESP) distribution of the C_3 isomer. Inset is the ESP calculated in the gas phase viewed from the side including a phenyl ring. Color scale from red to blue corresponds to negative to positive. In (a) and (b), C−F···π interaction is indicated by black arrows.

Figure 7 shows the proposed (4 × 4) supercell model and calculated electrostatic potential (ESP) distribution on the electron density surface of the C_3 isomer. The ESP around the phenyl ring was more positive (blue), and that around the fluorine atoms more negative (red). This suggests that there should be an attractive force due to the electrostatic interaction between the phenyl rings of a molecule and the fluorine atoms of neighboring molecules. It has been reported that the C−F···π interaction influences the 3D crystal packing of the fluorocarbon compounds.[17,21−24] In this model, the close-packed directions of the molecules correspond to ⟨110⟩ of the Au(111) beneath as explained previously. Another point to note is that the distance between the nearest neighbor F atoms at the bottom side (three green spheres in Figure 7a) is 0.29 and 0.28 nm according to the gas phase and periodic DFT calculation results, respectively, which is very close to the distance between the nearest neighbor atoms of the Au(111) surface; all three F atoms are thus considered to be at the same sites according to the highly symmetric STM images of molecules in the homogeneous region.

To orient molecules so that the C−F···π interaction is maximized, there is only one possible configuration: that shown in Figure 7 and Figure S4a. In this model, the center of the molecule is at the top site and the three F atoms nearest to the substrate are at bridge sites of Au(111). If the molecular center is located at a top site but the three F atoms are at hollow sites (Figure S4b), or if the center is at a hollow site and the F atoms are at either hollow sites (Figure S4c) or top sites (Figure S4d), the electrostatic interaction cannot be maximized. The adsorption site of F atoms in our model agrees with the case of halogen atoms adsorbed on the (111) surface of the face-centered-cubic (fcc) metal, where the preferential sites were found to be either bridge or 3-fold hollow sites.[41−43] The calculated optimized structure at the Au(111) top site (Figure S2a) fits this model well. Another possible model, shown in Figure S4b, is not allowed due to the steric hindrance between F atoms of neighboring molecules.

It is worth noting that $C_{60}F_{36}$ shows only one rotational domain because of the intermolecular C−F···π interaction, which is in contrast to C_{60}/Au(111), where several rotational orientations are possible as molecules interact with weaker van der Waals force.[25,26,44,45]

CONCLUSION

In conclusion, we have successfully formed a 2D $C_{60}F_{36}$ superstructure on Au(111) and investigated using STM and DFT calculations. Charge transfer due to strong electron-accepting ability and electrostatic C−F···π interaction among neighboring molecules allow $C_{60}F_{36}$ to adsorb in a specific orientation when enough thermal energy is provided. Analysis of the LUMO distribution strongly supports the formation of homogeneous regions with only one type of isomer, C_3, which suggests that the manipulation of the fluorination pattern may allow control over molecular orientation on the substrate. If the separation of isomers can be achieved and established, a complete monolayer of $C_{60}F_{36}$ on Au electrodes may be feasible. Such a film provides uniform electronic properties with a wide band gap with a deep HOMO and might be technologically relevant, for example, to electron transport layers in organic optoelectronic devices.

METHODS

Sample Preparation. Au(111) was prepared using cycles of Ar^+ ion sputtering and annealing. $C_{60}F_{36}$ (99% purity) purchased from Materials Technologies Research Ltd. contains three constitutional isomers: C_3, C_1, and T in the ratio of, approximately, C_3:C_1:T = 70:25:5 according to the specification data provided by the supplier. A homemade Knudsen cell (K-cell) was used for deposition. The temperature at the K-cell was raised to around 460 K, and the sample was kept at room temperature during deposition. For the formation of large homogeneous regions, the sample was annealed to 340−370 K after deposition.

STM Experiments. STM experiments were performed with a low-temperature STM system (Omicron) in an ultra-high-vacuum chamber. Base pressure was less than 5×10^{-11} Torr. All STM measurements were performed at 5 K. Bias was applied to the sample (V_{sample}). STS was acquired using a standard lock-in

technique with a bias modulation of 30 mV and 617 Hz while opening the feedback loop.

DFT Calculations. Isolated molecular geometries of three $C_{60}F_{36}$ isomers were fully optimized under C_3, C_1, and T symmetries, respectively, using DFT calculations. We employed B3LYP (Becke's three-parameter hybrid functional combined with the Lee−Yang−Parr correlation functional)[46] and 6-311+G(2d) basis set implemented in the Gaussian09 software package.[47] The EA values of $C_{60}F_{36}$ isomers were calculated and compared to that of the C_{60} molecule (Table S1), which are in good agreement with the experimental values.[6] Each anionic isomer was optimized without any symmetry restriction.

To investigate the adsorption behavior of the C_3 and T $C_{60}F_{36}$ isomers on Au(111) in more detail, we extended the computational study into periodic DFT calculations using the Vienna Ab initio Simulation Package (VASP) code.[48,49] The calculations were performed using the local density approximation for the exchange−correlation functional parametrized by Perdew and Zunger.[50] The core electrons were replaced by projector-augmented wave pseudopotentials[51,52] and expanded in a basis set of plane waves up to a cutoff energy of 400 eV. In accordance with the STM measurement, we used (4×4) surface supercells. The calculated fcc bulk lattice constant is 4.06 Å for Au, which agrees well with the experimental value (4.08 Å).[53] The slab model consists of six Au layers. The periodically replicated slabs were separated by a vacuum region of ~10 Å. During ionic relaxations, the two bottom Au layers were fixed in their bulk positions. Ionic relaxations were performed until atomic forces were less than 0.01 eV/Å. A $5 \times 5 \times 1$ Monkhorst−Pack k-point grid was used for Brillouin zone sampling.[54] Bader population analysis was performed to evaluate charge transfer between $C_{60}F_{36}$ and Au(111).[55] Dipole correction was applied in order to avoid interactions between periodic slab images. The symmetry of the structure was conserved during optimization where the periodic DFT calculations were performed without any symmetry restrictions. To explain the lateral orientation of $C_{60}F_{36}$ molecules due to intermolecular interaction, ESP maps were generated at both gas phase and periodic boundary conditions.

Conflict of Interest: The authors declare no competing financial interest.

Acknowledgment. This work is financially supported in part by a Grant-in-Aid for Scientific Research (S) "Single Molecule Spectroscopy Using Probe Microscope" from the Ministry of Education, Culture, Sports, Science and Technology (MEXT) of Japan. T.K.S. acknowledges financial support by the Sasakawa Scientific Research Grant from The Japan Science Society. We are grateful for the computational resources of the RIKEN Integrated Cluster of Clusters (RICC) supercomputer system. This work is also supported by a KBSI grant (T3109A) to Y.-K.H. We thank David W. Chapmon for carefully reading the manuscript.

Supporting Information Available: A large-scale STM image with different contrasts; the calculated density of states and LUMO+n spatial distributions for the C_3 and T isomers on Au(111); other superstructure models considered; the electron affinities, absolute energies, and optimized Cartesian coordinates of isolated $C_{60}F_{36}$ isomers; the optimized geometries and fractional coordinates for the C_3 and T isomers adsorbed on Au(111) obtained by periodic DFT calculations. This material is available free of charge *via* the Internet at http://pubs.acs.org.

REFERENCES AND NOTES

1. Tang, M. L.; Bao, Z. Halogenated Materials as Organic Semiconductors. *Chem. Mater.* **2011**, *23*, 446–455.
2. Babudri, F.; Farinola, G. M.; Naso, F.; Ragni, R. Fluorinated Organic Materials for Electronic and Optoelectronic Applications: The Role of the Fluorine Atom. *Chem. Commun.* **2007**, 1003–1022.
3. Taylor, R. Fluorinated Fullerenes. *Chem.—Eur. J.* **2001**, *7*, 4074–4083.
4. Kebarle, P.; Chowdhury, S. Electron Affinities and Electron-Transfer Reactions. *Chem. Rev.* **1987**, *87*, 513–534.
5. Kanai, K.; Akaike, K.; Koyasu, K.; Sakai, K.; Nishi, T.; Kamizuru, Y.; Nishi, T.; Ouchi, Y.; Seki, K. Determination of Electron Affinity of Electron Accepting Molecules. *Appl. Phys. A: Mater. Sci. Process.* **2009**, *95*, 309–313.
6. Boltalina, O. V.; Ponomarev, D. B.; Sidorov, L. N. Thermochemistry of Fullerene Anions in the Gas Phase. *Mass Spectrom. Rev.* **1997**, *16*, 333–351.
7. Sakamoto, Y.; Suzuki, T.; Kobayashi, M.; Gao, Y.; Fukai, Y.; Inoue, Y.; Sato, F.; Tokito, S. Perfluoropentacene: High-Performance p-n Junctions and Complementary Circuits with Pentacene. *J. Am. Chem. Soc.* **2004**, *126*, 8138–8140.
8. Strobel, P.; Riedel, M.; Ristein, J.; Ley, L. Surface Transfer Doping of Diamond. *Nature* **2004**, *430*, 439–441.
9. Strobel, P.; Riedel, M.; Ristein, J.; Ley, L.; Boltalina, O. Surface Transfer Doping of Diamond by Fullerene. *Diamond Relat. Mater.* **2005**, *14*, 451–458.
10. Sque, S. J.; Jones, R.; Öberg, S.; Briddon, P. R. Transfer Doping of Diamond: The Use of C_{60} and $C_{60}F_{36}$ to Effect p-Type Surface Conductivity. *Phys. B (Amsterdam, Neth.)* **2006**, *376−377*, 268–271.
11. Sque, S. J.; Jones, R.; Goss, J. P.; Briddon, P. R.; Öberg, S. First-Principles Study of C_{60} and $C_{60}F_{36}$ as Transfer Dopants for p-Type Diamond. *J. Phys.: Condens. Matter* **2005**, *17*, L21–L26.
12. Liu, N.; Morio, Y.; Okino, F.; Touhara, H. Electrochemical Properties of $C_{60}F_{36}$. *Synth. Met.* **1997**, *86*, 2289–2290.
13. Mikoushkin, V. M.; Shnitov, V. V.; Bryzgalov, V. V.; Gordeev, Yu. S.; Boltalina, O. V.; Gol'dt, I. V.; Molodtsov, S. L.; Vyalykh, D. V. Electronic Structure of Unoccupied States of Fluorinated Fullerenes $C_{60}F_{18}$ and $C_{60}F_{36}$. *Fullerenes Nanotubes Carbon Nanostruct.* **2008**, *16*, 588–592.
14. Mikoushkin, V. M.; Shnitov, V. V.; Bryzgalov, V. V.; Gordeev, Yu. S.; Boltalina, O. V.; Gol'dt, I. V.; Molodtsov, S. L.; Vyalikh, D. V. Valence Band Electronic Structure of $C_{60}F_{18}$ and $C_{60}F_{36}$ Studied by Photoelectron Spectroscopy. *J. Electron Spectrosc. Relat. Phenom.* **2008**, *168*, 25–28.
15. Reichenbächer, K.; Süss, H. I.; Hulliger, J. Fluorine in Crystal Engineering—"the Little Atom That Could". *Chem. Soc. Rev.* **2005**, *34*, 22–30.
16. Gakh, A. A.; Tuinman, A. A. The Structure of $C_{60}F_{36}$. *Tetrahedron Lett.* **2001**, *42*, 7133–7135.
17. Thilgen, C.; Diederich, F. Structural Aspects of Fullerene Chemistry—A Journey through Fullerene Chirality. *Chem. Rev.* **2006**, *106*, 5049–5135.
18. Wong, S. L.; Huang, H.; Huang, Y. L.; Wang, Y. Z.; Gao, X. Y.; Suzuki, T.; Chen, W.; Wee, A. T. S. Effect of Fluorination on the Molecular Packing of Perfluoropentacene and Pentacene Ultrathin Films on Ag(111). *J. Phys. Chem. C* **2010**, *114*, 9356–9361.
19. Wang, J.-Z.; Sadowski, J. T.; Xiong, Z.-H.; Fujikawa, Y.; Xue, Q. K.; Sakurai, T. Comparative Studies of Pentacene and Perfluoropentacene Grown on a Bi(0001) Surface. *Nanotechnology* **2009**, *20*, 095704.
20. Specification was provided by the supplier, Materials Research Technology Ltd.
21. Prasanna, M. D.; Guru Row, T. N. C−Halogen$\cdots\pi$ Interactions and Their Influence on Molecular Conformation and Crystal Packing: A Database Study. *Cryst. Eng.* **2000**, *3*, 135–154.
22. Bagryanskaya, I. Yu.; Gatilov, Y. V.; Maksimov, A. M.; Platonov, V. E.; Zibarev, A. V. Supramolecular Synthons in Crystals of Partially Fluorinated Fused Aromatics: 1,2,3,4-Tetrafluoronaphthalene and its Aza-analogue 1,3,4-Trifluoroisoquinoline. *J. Fluorine Chem.* **2005**, *126*, 1281–1287.
23. Rybalova, T. V.; Gatilov, Yu. V.; Sinyakov, V. R.; Mezhenkova, T. V.; Karpov, V. M. X-ray Diffraction Investigation of Perfluoro-4-methylenecyclohexa-2,5-dienones. *J. Struct. Chem.* **2008**, *49*, 125–130.
24. Rybalova, T. V.; Bagryanskaya, I. Yu. C-F$\cdots\pi$, F$\cdots$H, and F$\cdots$F Intermolecular Interactions and F-aggregation: Role in Crystal Engineering of Fluoroorganic Compounds. *J. Struct. Chem.* **2009**, *50*, 741–753.
25. Tang, L.; Xie, Y.; Guo, Q. Complex Orientational Ordering of C_{60} Molecules on Au(111). *J. Chem. Phys.* **2011**, *135*, 114702.

26. Gardener, J. A.; Briggs, G. A. D.; Castell, M. R. Scanning Tunneling Microscopy Studies of C_{60} Monolayers on Au(111). *Phys. Rev. B* **2009**, *80*, 235434.
27. Wong, S. L.; Huang, H.; Wang, Y.; Cao, L.; Qi, D.; Santoso, I.; Chen, W.; Wee, A. T. S. Quasi-Free-Standing Epitaxial Graphene on SiC(0001) by Fluorine Intercalation from a Molecular Source. *ACS Nano* **2011**, *5*, 7662–7668.
28. Fujikawa, Y.; Sadowski, J. T.; Kelly, K. F.; Nakayama, K. S.; Mickelson, E. T.; Hauge, R. H.; Margrave, J. L.; Sakurai, T. Adsorption of Fluorinated C_{60} on the Si(111)-(7×7) Surface Studied by Scanning Tunneling Microscopy and High-Resolution Electron Energy Loss Spectroscopy. *Jpn. J. Appl. Phys.* **2002**, *41*, 245–249.
29. Bakhtizin, R. Z.; Oreshkin, A. I.; Murugan, P.; Kumar, V.; Sadowski, J. T.; Fujikawa, Y.; Kawazoe, Y.; Sakurai, T. Adsorption and Electronic Structure of Single $C_{60}F_{18}$ Molecule on Si(111)-7×7 Surface. *Chem. Phys. Lett.* **2009**, *482*, 307–311.
30. Tzeng, C.-T.; Lo, W.-S.; Yuh, J.-Y.; Chu, R.-Y.; Tsuei, K.-D. Photoemission, Near-Edge X-ray-absorption Spectroscopy, and Low-Energy Electron-Diffraction Study of C_{60} on Au(111) Surfaces. *Phys. Rev. B* **2000**, *61*, 2263–2272.
31. Park, B. K.; Lee, C. Y.; Jung, J.; Lim, J. H.; Han, Y.-K.; Hong, C. S.; Park, J. T. $[Os_3(CO)_6(PMe_3)_3](\mu_3\text{-}\eta^2\text{:}\eta^2\text{:}\eta^2\text{-}C_{60})[Re_3(\mu\text{-}H)_3(CO)_9]$: A Fullerene[60] Coordinated to Two Different Trinuclear Clusters. *Angew. Chem., Int. Ed.* **2007**, *46*, 1436–1439.
32. Rangger, G. M.; Hofmann, O. T.; Romaner, L.; Heimel, G.; Bröker, B.; Blum, R.-P.; Johnson, R. L.; Koch, N.; Zojer, E. F4TCNQ on Cu, Ag, and Au as Prototypical Example for a Strong Organic Acceptor on Coinage Metals. *Phys. Rev. B* **2009**, *79*, 165306.
33. Lei, S.-B.; Deng, K.; Yang, D.-L.; Zeng, Q.-D.; Wang, C. Charge-Transfer Effect at the Interface of Phthalocyanine–Electrode Contact Studied by Scanning Tunneling Spectroscopy. *J. Phys. Chem. B* **2006**, *110*, 1256–1260.
34. Toader, M.; Gopakumar, T. G.; Shukrynau, P.; Hietschold, M. Exploring the F_{16}CoPc/Ag(110) Interface Using Scanning Tunneling Microscopy and Spectroscopy. 2. Adsorption-Induced Charge Transfer Effect. *J. Phys. Chem. C* **2010**, *114*, 21548–21554.
35. Rogero, C.; Pascual, J. I.; Gómez-Herrero, J.; Baró, A. M. Resolution of Site-Specific Bonding Properties of C_{60} Adsorbed on Au(111). *J. Chem. Phys.* **2002**, *116*, 832–836.
36. Yang, Y.-C.; Chang, C.-H.; Lee, Y.-L. Complexation of Fullerenes on a Pentacene-Modified Au(111) Surface. *Chem. Mater.* **2007**, *19*, 6126–6130.
37. Alkauskas, A.; Baratoff, A.; Bruder, C. Site-Selective Adsorption of Naphthalene-tetracarboxylic-dianhydride on Ag(110): First-Principles Calculations. *Phys. Rev. B* **2006**, *73*, 165408.
38. Song, F.; Dou, W.; Huang, H.; Li, H.; He, P.; Bao, S.; Chen, Q.; Zhou, W. The Adsorption with Chiral Structure of Fluorene-1-carboxylic Acid Molecules on Cu(110) Surface. *Chem. Phys. Lett.* **2008**, *452*, 275–280.
39. Mugarza, A.; Lorente, N.; Ordejón, P.; Krull, C.; Stepanow, S.; Bocquet, M.-L.; Fraxedas, J.; Ceballos, G.; Gambardella, P. Orbital Specific Chirality and Homochiral Self-assembly of Achiral Molecules Induced by Charge Transfer and Spontaneous Symmetry Breaking. *Phys. Rev. Lett.* **2010**, *105*, 115702.
40. Wang, L.-L.; Cheng, H.-P. Density Functional Study of the Adsorption of a C_{60} Monolayer on Ag(111) and Au(111) Surfaces. *Phys. Rev. B* **2004**, *69*, 165417.
41. Schott, J. H.; White, H. S. Halogen Adlayers on Ag(111). *J. Phys. Chem.* **1994**, *98*, 291–296.
42. Magnussen, O. M. Ordered Anion Adlayers on Metal Electrode Surfaces. *Chem. Rev.* **2002**, *102*, 679–725.
43. Pašti, I. A.; Mentus, S. V. Halogen Adsorption on Crystallographic (111) Planes of Pt, Pd, Cu and Au, and on Pd-monolayer Catalyst Surfaces: First-Principles Study. *Electrochim. Acta* **2010**, *55*, 1995–2003.
44. Schull, G.; Berndt, R. Orientationally Ordered (7×7) Superstructure of C_{60} on Au(111). *Phys. Rev. Lett.* **2007**, *99*, 226105.
45. Zhang, X.; Yin, F.; Palmer, R. E.; Guo, Q. The C_{60}/Au(111) Interface at Room Temperature: A Scanning Tunnelling Microscopy Study. *Surf. Sci.* **2008**, *602*, 885–892.
46. Becke, A. D. Density-functional Thermochemistry. III. The Role of Exact Exchange. *J. Chem. Phys.* **1993**, *98*, 5648–5652.
47. Frisch, M. J.; Trucks, G. W.; Schlegel, H. B.; Scuseria, G. E.; Robb, M. A.; Cheeseman, J. R.; Scalmani, G.; Barone, V.; Mennucci, B.; Petersson, G. A.; *et al. Gaussian 09*, Revision B.1; Gaussian, Inc.: Wallingford, CT, 2010.
48. Kresse, G.; Hafner, J. *Ab Initio* Molecular Dynamics for Liquid Metals. *Phys. Rev. B* **1993**, *47*, 558–561.
49. Kresse, G.; Furthmüller, J. Efficient Iterative Schemes for *Ab Initio* Total-Energy Calculations Using a Plane-Wave Basis Set. *Phys. Rev. B* **1996**, *54*, 11169–11186.
50. Perdew, J. P.; Zunger., A. Self-Interaction Correction to Density-Functional Approximations for Many-Electron Systems. *Phys. Rev. B* **1981**, *23*, 5048–5079.
51. Blöchl, P. E.; Jepsen, O.; Andersen, O. K. Improved Tetrahedron Method for Brillouin-Zone Integrations. *Phys. Rev. B* **1994**, *49*, 16223–16233.
52. Kresse, G.; Joubert, D. From Ultrasoft Pseudopotentials to the Projector Augmented-Wave Method. *Phys. Rev. B* **1999**, *59*, 1758–1775.
53. Maeland, A.; Flanagan, T. Lattice Spacings of Gold-Palladium Alloys. *Can. J. Phys.* **1964**, *42*, 2364–2366.
54. Monkhorst, H. J.; Pack, J. D. Special Points for Brillouin-Zone Integrations. *Phys. Rev. B* **1976**, *13*, 5188–5192.
55. Tang, W.; Sanville, E.; Henkelman, G. A Grid-Based Bader Analysis Algorithm without Lattice Bias. *J. Phys.: Condens. Matter* **2009**, *21*, 084204.